

Slow rupture of frictional interfaces

Yohai Bar Sinai¹, Efim A. Brener^{1,2} and Eran Bouchbinder¹

¹ *Chemical Physics Department, Weizmann Institute of Science, Rehovot 76100, Israel*

² *Peter Grünberg Institut, Forschungszentrum Jülich, Jülich 52425 Germany*

The failure of frictional interfaces and the spatio-temporal structures that accompany it are central to a wide range of geophysical, physical and engineering systems. Recent geophysical and laboratory observations indicated that interfacial failure can be mediated by slow slip rupture phenomena which are distinct from ordinary, earthquake-like, fast rupture. These discoveries have influenced the way we think about frictional motion, yet the nature and properties of slow rupture are not completely understood. We show that slow rupture is an intrinsic and robust property of simple non-monotonic rate-and-state friction laws. It is associated with a new velocity scale c_{min} , intrinsically determined by the friction law, below which steady state rupture cannot propagate. We further show that rupture can occur in a continuum of states, spanning a wide range of velocities from c_{min} to elastic wave-speeds, and predict different properties for slow rupture and common fast rupture. Our results are in qualitative agreement with recent high-resolution laboratory measurements and may provide a theoretical framework for understanding slow rupture phenomena along frictional interfaces.

I. INTRODUCTION

Understanding the dynamic processes that govern interfacial failure and frictional sliding, e.g. a large earthquake along a natural fault, remains a major scientific challenge. Quite recently, several geophysical and high-resolution real-time laboratory observations have pointed to the possibility that stress releasing interfacial slip can be mediated by the propagation of rupture fronts whose velocity is much smaller than elastic wave-speeds [1–5]. These slow rupture fronts typically radiate seismic energy at significantly reduced rates and hence are less destructive than ordinary earthquakes. Furthermore, the propagation of slow rupture fronts was observed to precede major slip events, possibly during the nucleation and early stages of large scale rupture, and hence raised some interest in their potential predictive roles.

The nature and properties of these slow rupture fronts, and in particular their propagation velocity, are still not fully understood. The experiments of [1, 5] clearly demonstrate the existence of a minimal propagation velocity below which no fronts are observed. To the best of our knowledge, no theoretical understanding of this minimal velocity is currently available.

Frictional phenomena is commonly described using phenomenological rate-and-state friction models [6–8]. Two possible mechanisms for generating slow rupture events were invoked in this framework. The first involves a non-monotonic dependence of the steady state frictional resistance on slip velocity [9–11], while the second involves spatial variation of friction parameters and the accompanying heterogeneous stress distribution [12, 13]. The former mechanism is an intrinsic property of the friction law, while the latter mechanism is an extrinsic one. The high-resolution laboratory measurements of [1, 5, 14], performed on a quasi-2D spatially homogeneous system, suggests that the second mechanism is not necessary for the existence of slow rupture.

In this Letter we show that slow rupture naturally emerges in the framework of spatially homogeneous rate-

and-state friction models. Our analysis is based on a friction model that includes an elastic response at small shear stresses and a transition to slip above a threshold stress, following the “minimal” microscopic model of [15] and its continuum generalization [16]. The model exhibits a crossover from velocity-weakening friction at small slip rates to velocity-strengthening friction at higher slip rates, which we argue to be a generic feature of friction.

The existence of a minimal rupture front velocity c_{min} , which is determined by the friction law and is independent of elastic wave-speeds, is predicted analytically in a quasi-1D limit. We show that there exists a continuum of rupture fronts with velocities ranging between c_{min} and elastic wave-speeds, in qualitative agreement with recent laboratory measurements [1] and consistent with field observations [4]. We further show that slow rupture is significantly less spatially localized than ordinary fast rupture. These predictions are corroborated by explicit calculations for a glassy polymer that was extensively used in laboratory experiments [1, 5, 14, 17], demonstrating the existence of slow rupture which is well-separated from ordinary fast rupture. We propose that these results are possibly relevant for slow/silent earthquakes in geological contexts.

II. A RATE-AND-STATE FRICTION MODEL

Our goal here is to further develop and incorporate the ideas discussed recently in [15, 16, 18] into a realistic rate-and-state friction model. We consider a spatially extended interface between macroscopic bodies in frictional contact. The interface is composed of an ensemble of contact asperities whose total area A_r is much smaller than the nominal contact area A_n and which exert a shear stress τ that resists sliding motion. We decompose τ into an elastic part, emerging from the elastic deformations of contact asperities which are characterized by a

coarse-grained stress τ^{el} , and a viscous part τ^{vis}

$$\tau = \tau^{el} + \tau^{vis} = \tau^{el} + \eta v^* A \operatorname{sgn}(v) \log \left(1 + \frac{|v|}{v^*} \right), \quad (1)$$

where η is a viscous-friction coefficient, v is the slip velocity (rate), v^* is a reference velocity scale and $A = A_r/A_n \ll 1$ is the normalized real contact area. The viscous-stress τ^{vis} , which increases with v and scales with A , is usually associated with activated rate processes at asperity contacts [8]. The 1 inside the log ensures a regular behavior in the limit $v \rightarrow 0$, but otherwise does not play a crucial role in what follows.

The next step is writing down a dynamic evolution equation for τ^{el} . τ^{el} is stored at contact asperities at a rate determined by v and is proportional to both the interfacial elastic modulus μ_0 and A . It is released as contact asperities are destroyed after slipping over a typical distance D (of the order of the size of a contact), when the asperity-level stress surpasses a yield-like threshold τ_c . This physical picture is mathematically captured by writing [16]

$$\dot{\tau}^{el} = \frac{\mu_0 A}{h} v - \frac{\tau^{el} |v|}{D} \theta \left(\frac{\tau}{A} - \tau_c \right), \quad (2)$$

where h is the asperities' effective height. Note that the coarse-grained stress τ is enhanced by a factor $A^{-1} \gg 1$ at the asperities level and that the geometric nature of elastic stress relaxation, emerging from the multi-contact nature of the interface, is captured by the introduction of a spatial length D , that is interpreted as the typical size of a contact as in conventional rate-and-state models [6–8]. The appearance of a step function non-linearity $\theta(\cdot)$ is an outcome of the basic notion of a static threshold for sliding motion. The evolution law in Eq. (2) features a reversible elastic response at small shear stresses, $\tau \simeq \tau^{el} = \mu_0 A u/h$, where u is the shear displacement. This elastic response is usually not included in friction models (but see [19, 20]), even though it was directly measured experimentally [17]. We will later use these experimental data to constrain parameters such as μ_0/h .

To proceed, we write the normalized contact area A in terms of a state variable ϕ ,

$$A(\phi, \sigma) = A_0(\sigma) [1 + b \log(1 + \phi/\phi_0)]. \quad (3)$$

Here σ is the (compressive) normal stress and $A_0(\sigma) = \sigma/\sigma_H$, where σ_H is the hardness. The evolution of the contact area is phenomenologically determined from two robust observations: logarithmic aging in the absence of irreversible slip and a logarithmic velocity-weakening steady-state behavior [8]. This is commonly captured by Dieterich's evolution law [6], extended here by stipulating that the transition from the aging regime ($v=0$) to the sliding regime ($v \neq 0$) is controlled by the same step function nonlinearity as in equation (2), yielding

$$\dot{\phi} = 1 - \frac{\phi |v|}{D} \theta \left(\frac{\tau}{A} - \tau_c \right), \quad (4)$$

where ϕ is interpreted as the “geometric age” of the contacts. Equations (1)–(4) determine the evolution of $\tau(t)$, i.e. constitute our proposed friction law.

Before we proceed we note a very important feature of rate-and-state friction models, which is not specific to the present model. In the absence of persistent sliding, $v=0$, we have $\phi=t$ and the contact area ages logarithmically $A \propto 1 + b \log(1+t/\phi_0)$, as is widely observed [8]. The latter form suggests that the logarithmic law is cutoff at short timescales, smaller than ϕ_0 , as was directly confirmed experimentally [14, 21]. This very same short timescales cutoff manifests itself also under persistent sliding, $v \neq 0$, for which we have $\phi = D/|v|$ and $A \propto 1 + b \log[1 + D/(\phi_0|v|)]$. In this case, A saturates at a finite value above a typical slip rate of order D/ϕ_0 and the fixed-point of Eq. (2), $\tau^{el} \propto A$, becomes v -independent as well. As a consequence, τ , which usually exhibits a velocity-weakening behavior at small v , becomes velocity-strengthening as the viscous-friction term in Eq. (1) takes over. Thus, rate-and-state friction models generically predict a non-monotonic dependence of the steady state sliding friction on the slip rate, an observation that has been largely overlooked in the literature (but see [8, 10, 11, 22]) and that will play an important role below.

III. STEADY STATE RUPTURE FRONTS

At this point we are interested in steady state propagating front solutions corresponding to our friction law. Such propagating solutions exist in multi-stable systems in which one homogeneous (space independent) solution invades another one, giving rise to non-trivial spatiotemporal structures. The spatially homogeneous solutions of equations (1)–(4), as a function of a driving stress τ^d , are shown in Fig. 1a. A branch of elastic (static) solutions exists at $v=0$, where aging effects are neglected, i.e. we assume that $\psi_0 \equiv b \log(1+t/\phi_0)$ is roughly constant for the timescales relevant for front propagation. A branch of steady sliding solutions with $v>0$ takes the form

$$f = \frac{\tau_{ss}}{\sigma} \simeq f_0 + \alpha \log \left(1 + \frac{v}{v^*} \right) + \beta \log \left(1 + \frac{D}{\phi_0 v} \right), \quad (5)$$

where

$$\alpha \equiv \eta v^*/\sigma_H, \quad \beta \equiv \mu_0 D b/\sigma_H h, \quad f_0 \equiv \beta/b, \quad (6)$$

and f is the steady sliding friction coefficient. Note that we neglected a term of order \log^2 in Eq. (5). As discussed above, steady sliding friction is indeed non-monotonic (when $\alpha < \beta$); friction is velocity-weakening for $v^* \ll v \ll D/\phi_0$ and velocity-strengthening for $v \gg D/\phi_0$, with a minimum at

$$v_m \simeq \frac{\beta - \alpha}{\alpha} \frac{D}{\phi_0}. \quad (7)$$

At the minimum, we define the friction stress as $\tau_m = \tau_{ss}(v_m)$. Figs. 1b-d present experimental data for three

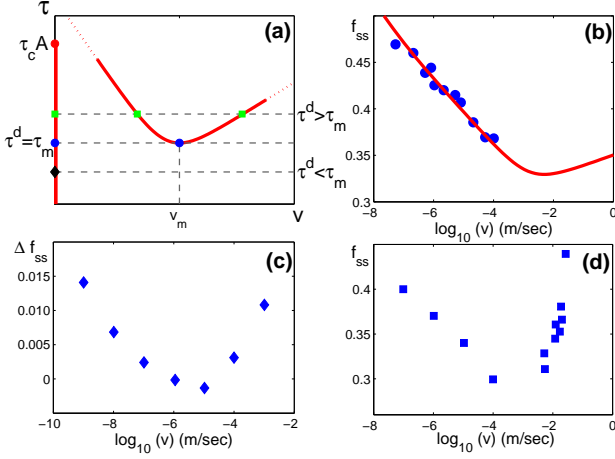


FIG. 1: (a) A schematic sketch of the homogeneous solutions of $\tau(v)$. The elastic (static) branch is shown as a vertical line at $v=0$, which ends at the threshold $\tau_c A$. The non-monotonic steady sliding curve is shown at $v>0$. The slip velocity at the minimum is denoted by v_m and the corresponding steady state friction stress by τ_m . The horizontal dashed lines denote different levels of the driving stress τ^d with respect to τ_m and the corresponding homogeneous solutions (filled symbols). (b) The steady sliding friction coefficient $f(v)$ for PMMA [23]. The solid line is a fit to Eq. (5). This fit was highly constrained by additional independent data sets, see Sect. IV. (c) $\Delta f(v)$ (defined with respect to some reference level) for granite with $\sigma=5$ MPa [24]. (d) $f(v)$ for paper [25].

different materials, where the last two data sets clearly demonstrate the non-monotonic nature of sliding friction, and the first one presumably does not span a sufficiently large range of v 's to detect a minimum.

Consider now a homogeneous driving stress τ^d . For $\tau^d < \tau_m$ there exists only one stable homogeneous solution, the elastic (static) one. Upon increasing τ^d above τ_m , three solutions exist: the elastic one with $v=0$ and two steady sliding solutions, one with $v < v_m$ (typically unstable) and one with $v > v_m$ (typically stable). The critical point $\tau^d = \tau_m$ corresponds to a bifurcation, which suggests a qualitative change in the behavior of the system. At this point we expect steady state propagating rupture, in which a solution with $v \geq v_m$ invades an elastic (static) solution with $v=0$, to emerge. Denote the propagation velocity of such fronts by c and the one corresponding to $\tau^d = \tau_m$ by c_{min} .

In order to find propagating rupture solutions, and in particular to calculate c_{min} , we need to couple the friction law in Eqs. (1)-(4) to an elastic body. It would be very difficult to analytically calculate c_{min} when the body is a 2D medium. Therefore, to gain analytic insight into the properties of the steady state fronts, we assume that the height H of the elastic body (say in the y -direction) is much smaller than the spatial scale of variation ℓ of fields along the interface (in the x -direction), i.e. we consider a quasi-1D limit. Under these condi-

tions, integrating the bulk momentum balance equation, $\rho \partial_{tt} u_i = \partial_j \sigma_{ij}$ (where ρ is the bulk mass density, σ_{ij} are the stress components and u_i are the displacement components) along the y -direction yields

$$H \rho \partial_{tt} u(x, t) \simeq H \mu \partial_{xx} u(x, t) + \tau^d - \tau(x, t), \quad (8)$$

where μ is the bulk shear modulus and $u = u_x$ is the interfacial shear displacement (slip) that satisfies $\partial_t u = v$. Note that we have omitted constants of order unity in Eq. (8) and that in the quasi-1D limit both the driving stress τ^d and the friction stress τ do not appear as boundary conditions, but rather as terms in the “bulk” equation.

We now look for steady state propagating solutions of Eqs. (2), (4) and (8) in which all of the fields take the form $g(\xi)$, with $\xi = x - ct$, such that a sliding solution at $\xi \rightarrow -\infty$ propagates into an elastic solution at $\xi \rightarrow \infty$. Smoothly connecting these two different solutions around $\xi=0$ provides solvability conditions that allow the calculation of c . Since the front propagation transforms an elastic region with high contact area to a sliding region with lower contact area, these are actually rupture fronts.

c_{min} is being estimated using a scaling calculation in which the loading τ^d is homogeneous and equals to its threshold value τ_m . A self-consistency constraint on the quasi-1D formulation is $H \ll \ell$, where ℓ is the spatial scale characterizing all of the fields in the front solution (as defined above). We first use $\partial_t = -c \partial_\xi$ to transform Eqs. (2), (4) and (8) into the following set of coupled ordinary differential equations

$$H \left(\frac{\mu}{c} - c \rho \right) \partial_\xi v = \tau^d - \tau, \quad (9)$$

$$-c \partial_\xi \tau^{el} = \frac{\mu_0}{h} A(\phi, \sigma) v - \frac{|v|}{D} \tau^{el} \theta \left(\frac{\tau}{A} - \tau_c \right), \quad (10)$$

$$-c \partial_\xi \phi = 1 - \frac{\phi |v|}{D} \theta \left(\frac{\tau}{A} - \tau_c \right). \quad (11)$$

We stress that the front velocity c in these equations is not a-priori known, but is rather a “nonlinear eigenvalue” of this problem. It is determined from the condition that the spatially-varying propagating solution properly converges to the homogeneous sliding solution at $\xi \rightarrow -\infty$ and to the homogeneous elastic solution at $\xi \rightarrow \infty$.

To proceed, we estimate the right-hand-side of Eq. (10) as $-v_m \tau^{el}/D$ and the left-hand-side as $-c_{min} \tau^{el}/\ell(c_{min})$, yielding

$$\ell(c_{min}) \sim D c_{min} / v_m. \quad (12)$$

We neglect inertia (i.e. assume $c_{min} \ll c_s = \sqrt{\mu/\rho}$) and estimate the left-hand-side of Eq. (9) as $-H \mu v_m / \ell(c_{min}) c_{min}$. For the right-hand-side, we estimate $\tau = \tau^{el} + \tau^{vis}$ by its peak value. The maximum of τ^{el} is obtained by solving Eq. (10) with $\partial_\xi \tau^{el} = 0$ to get $\tau_{max}^{el} \sim \mu_0 D A_0 (1 + \psi_0) / h$. We estimate that this happens roughly half-way through the front, i.e. $\xi \sim -\ell(c_{min})/2$ and $v \sim v_m/2$, so the viscous stress is $\tau^{vis} \sim \eta v^* \log(v_m/2v^*)$, where we used $v_m/v^* \gg 1$. Therefore,

we estimate $\tau \sim \mu_0 D A_0 (1 + \psi_0) / h + \eta v^* \log(v_m / 2v^*)$ and use $\tau^d = \tau_m \sim A_0 [\mu_0 D / h + \eta v^* \log(v_m / v^*)]$ to obtain a scaling version of Eq. (9). The result, together with Eq. (12), leads to the following prediction

$$c_{min} \sim v_m \sqrt{\frac{\mu H \sigma_H}{\sigma D [\mu_0 D \psi_0 / h - \eta v^* \log(2)]}}, \quad (13)$$

where we remind the reader that ψ_0 quantifies the typical age of the interface in the elastic regime prior to slip (see above).

Several features of this central result are noteworthy. First, c_{min} is finite and proportional to v_m . Second, it is independent of inertia, i.e. it does not scale with the elastic wave speed $c_s = \sqrt{\mu/\rho}$ [18]. Finally, c_{min} depends on: (i) the properties of the friction law, e.g. on constitutive parameters such as the viscous-friction coefficient η and the interfacial elastic modulus μ_0 and on microscopic geometric quantities such as D and h , (ii) the bulk geometry through H , (iii) the normal stress as $\sigma^{-1/2}$ and (iv) the bulk shear modulus μ . We expect these features to remain qualitatively valid independently of the explicit form of the friction law and of dimensionality as long as steady sliding friction exhibits a non-monotonic behavior (cf. Fig. 1a), as suggested in [16].

IV. AN EXPLICIT EXAMPLE

In order to test the prediction in Eq. (13) we should determine the friction parameters for a specific material. We focus on a glassy polymer (PMMA) which was extensively characterized in laboratory measurements, including the interfacial elastic response [17]. It was used in the most conclusive experiments which demonstrated the existence of slow rupture modes [1, 5].

μ	3.1 GPa	τ_c	130 MPa
σ_H	540 MPa	b	0.075
ρ	1,200 Kg/m ³	D	0.5 μm
v^*	0.1 $\mu\text{m}/\text{sec}$	D/ϕ_0	1.5 mm/sec
η	27 MPa ($\mu\text{m}/\text{s}$) ⁻¹	μ_0/h	300 MPa/ μm

TABLE I: Elastic and frictional parameters for PMMA.

We extracted the material parameters of PMMA from various sources. It seems that frictional parameters are sensitive to environmental and experimental conditions. Somewhat different results for (supposedly) the same material, sometimes by the same research group, were reported. However, the trends are robust, as well as the order of magnitude of the parameters. With this in mind, we compiled a list of parameters with which our model satisfactorily describes the data from all of the reported sources.

The interfacial elastic response data of Fig. 2 in [17] indicates that $h\sigma_H/\mu_0$ is in the μm scale. The slope of the

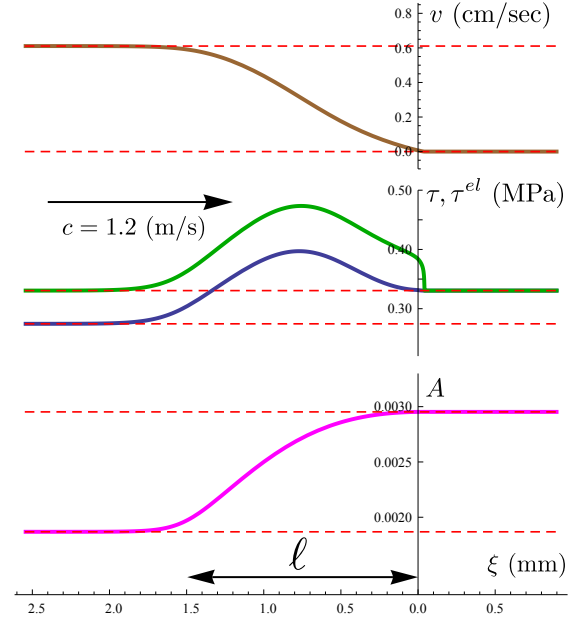


FIG. 2: From top to bottom, $v(\xi)$, $\tau(\xi)$, $\tau^{el}(\xi)$ and $A(\xi)$ for a steady state rupture mode propagating from left to right at 1.2 m/sec $\ll c_s$. The parameters for PMMA were used together with $\tau^d = \tau_m$. The spatial scale of variation of the fields is denoted by ℓ . The homogeneous states that the rupture mode smoothly connects are marked by horizontal dashed lines.

ageing data in Fig. 9 of [8] implies $\beta = \mu_0 D b / \sigma_H h \simeq 0.02$. The “direct effect” measurement in Fig. 4 of [8] implies $\alpha = \eta v^* / \sigma_H \simeq 0.005$. v^* was estimated as the lowest slip rate for which the logarithmic “direct effect” is observed. The data presented in Fig. 1b above are consistent with $\beta - \alpha \simeq 0.015$. D was determined to be 0.9 μm in [14] and 0.4 μm in [20]. With these constraints, and using known values of independently measured parameters such as μ , σ_H , ρ and τ_c (which is estimated as the yield stress), we fitted all of the aforementioned experimental data. The parameters are summarized in Table I. In addition, we set $\sigma = 1$ MPa, which is similar to the value used in [1, 14], $H = 10 \mu\text{m}$ and $\psi_0 = 0.6$.

In Fig. 2 we show a steady state rupture solution obtained by numerically integrating our model equations in (9)-(11) using these parameters and the threshold driving stress $\tau^d = \tau_m$. The front propagation velocity at threshold, $c_{min} = 1.2$ m/sec, is more than three orders of magnitude smaller than $c_s \approx 1,600$ m/sec, qualifying it as “slow rupture”, and $\ell(c_{min})$ is on a mm scale, satisfying $H \ll \ell$ as required by self-consistency.

We test the prediction in Eq. (13) by each time varying one parameter on the right-hand-side over a wide range and comparing the prediction to the numerically calculated c_{min} . The results are presented in Fig. 3 and exhibit excellent agreement between the analytic prediction and the numerically calculated values of c_{min} . This result clearly and directly demonstrates the existence of friction-controlled slow rupture in our model.

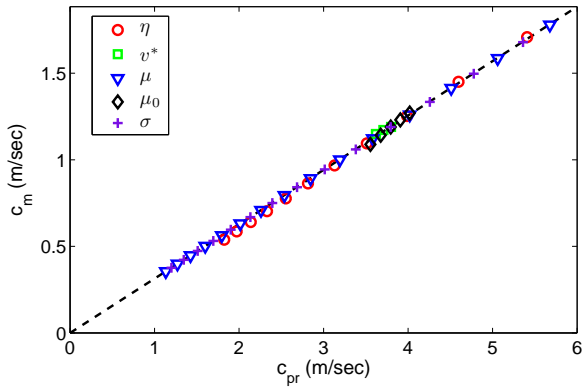


FIG. 3: The numerically calculated c_{min} vs. the analytic prediction appearing on the right-hand-side of equation (13), which we denote here as c_{pr} . Different symbols correspond to variations of different parameters of the model, as denoted in the legend. The dashed line serves as a guide to the eye.

V. THE SPECTRUM OF RUPTURE FRONTS

The finite velocity scale c_{min} implies there are no solutions with $c < c_{min}$, i.e. the existence of a “forbidden” range of velocities in the spectrum of steady state rupture modes [16]. In Fig. 4a we show the full spectrum of rupture propagation velocities as a function of $\tau^d \geq \tau_m$. Indeed, there are no solutions with $c < c_{min}$ and there exists a continuum of states between c_{min} and the elastic wave speed c_s . This continuous spectrum qualitatively agrees with recent high-resolution laboratory measurements [1], reproduced here in Fig. 4b. These measurements, though not obtained under globally homogeneous loading and were done in 2D, directly demonstrate the existence of a threshold driving stress, a minimal slow rupture velocity and saturation at an elastic wave speed. A detailed quantitative comparison to the experiments requires fully 2D calculations which are currently underway and will be reported elsewhere.

Upon increasing τ^d sufficiently above τ_m , rupture travels at a non-negligible fraction of the sound speed and we can no longer neglect the inertial term in Eq. (9). The sliding velocity in the sliding region of a propagating rupture solution corresponds to the larger v of the two solutions of $\tau^d = f(v)\sigma$, where $f(v)$ is given in Eq. (5). For $v \gg v_m$ it reads $v \sim v^* \exp(\tau^d/\alpha\sigma - \beta/\alpha b)$. The analog of relation (12) for the inertial regime, $c \sim c_s \gg c_{min}$, reads $\ell(c \sim c_s) \sim Dc/v$, which immediately implies

$$\ell(c \sim c_s) \sim e^{-\tau^d/\alpha\sigma} \ll \ell(c_{min}). \quad (14)$$

The strong inequality results from the exponential decay of $\ell(c)$ with τ^d in the inertial regime and the typically small value of α (~ 0.01 , see above). This result predicts that slow rupture is much less spatially localized as compared to ordinary fast rupture. To test this prediction we plot in Fig. 4c ℓ vs. τ^d/τ_m (which can be readily

converted into $\ell(c)$ using the results of Fig. 4c). The numerical results clearly confirm the theoretical prediction, demonstrating that indeed slow rupture is significantly less localized than rupture at elastodynamic velocities. Furthermore, the exponential dependence predicted in Eq. (14) is quantitatively verified and the slope agrees with $-1/\alpha\sigma$ to within a few percent. These predictions should be tested experimentally.

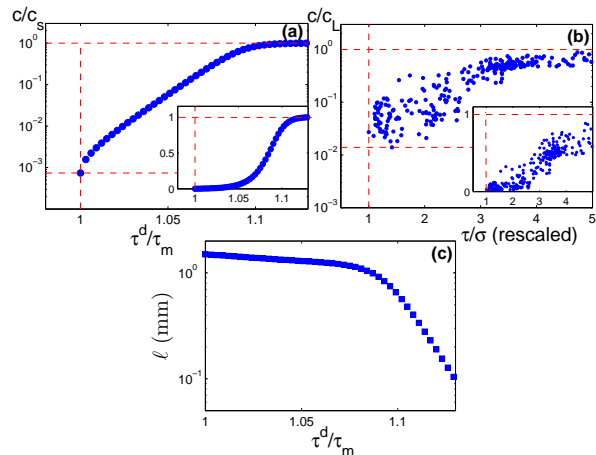


FIG. 4: (a) Semi-logarithmic plot of c/c_s vs. τ^d/τ_m , for a fixed σ . The same results are shown in linear-linear scale in the inset. The horizontal dashed lines denote c_{min} and $c_s \gg c_{min}$, and the vertical dashed line denotes the minimal driving stress $\tau^d = \tau_m$. (b) Semi-logarithmic plot of c/c_L vs. τ/σ in the PMMA experiments of [1] (data courtesy of O. Ben-David and J. Fineberg). The same data are shown in linear-linear scale in the inset. c_L is the longitudinal wave-speed and τ/σ is rescaled such that the minimal value below which no rupture modes were observed equals unity. c_{min} in the experiment was of the order of 10 m/sec. (c) Semi-logarithmic plot of ℓ vs. τ^d/τ_m for the spectrum shown in panel (a).

VI. SUMMARY AND CONCLUSIONS

Our results, based on a rate-and-state type friction law, show that slow rupture is a well-defined and generic state of frictional interfaces. The non-monotonic dependence of the steady state sliding friction on the slip velocity is shown to be directly related to the emergence of a new, friction-controlled, velocity scale c_{min} below which no steady state rupture can propagate. Furthermore, our analysis demonstrates that rupture states span a continuum, from friction-controlled slow rupture to inertia-limited, earthquake-like, fast rupture [4]. We suspect that transient rupture modes observed under complex, spatially inhomogeneous, conditions are short-lived excitations of these steady rupture states, as was argued and demonstrated in a specific context in [16]. If true, steady state rupture fronts play a role analogous to “normal modes” or “eigenstates” in other dynamical contexts.

The results presented were shown to be in qualitative agreement with the recent high-resolution real-time laboratory measurements of [1, 5]. A quantitative comparison to the experimental data requires 2D calculations which are currently underway. We believe that the developed ideas are applicable to geophysical systems, though such questions go well beyond the scope of the present work. The possible geophysical relevance of our results (e.g. to slow/silent earthquakes) should be carefully examined in a future investigation.

Acknowledgments

We thank O. Ben-David and J. Fineberg for numerous insightful discussions. EB acknowledges support of the James S. McDonnell Foundation, the Harold Perlman Family Foundation and the William Z. and Eda Bess Novick Young Scientist Fund. EAB acknowledges support of the Erna and Jacob Michael visiting professorship funds at Weizmann Institute of Science.

-
- [1] Ben-David, O., G. Cohen, and J. Fineberg, The dynamics of the onset of frictional slip, *Science*, *330*(6001), 211–214, 2010.
 - [2] Ide, S., Beroza, G. C., Shelly, D. R., and Uchide, T., A scaling law for slow earthquakes, *Nature*, *447*, 76–79, 2007.
 - [3] Nielsen, S., J. Taddeucci, and S. Vinciguerra, Experimental observation of stick-slip instability fronts, *Geophysical Journal International*, *180*(2), 697–702, 2010.
 - [4] Peng, Z., and Gomberg, J., An integrated perspective of the continuum between earthquakes and slow-slip phenomena, *Nature Geoscience*, *3*(9), 599–607, 2010.
 - [5] Rubinstein, S. M., G. Cohen, and J. Fineberg, Detachment fronts and the onset of dynamic friction, *Nature*, *430*(August), 1005–1009, 2004.
 - [6] Dieterich, J. H., Modeling of rock friction .1. Experimental results and constitutive equations, *Journal of Geophysical Research*, *84*, 2161–2168, 1979.
 - [7] Ruina, A., Slip instability and state variable friction laws, *Journal of Geophysical Research*, *88*, 10359–10370, 1983.
 - [8] Baumberger, T., and C. Caroli, Solid friction from stick-slip down to pinning and aging, *Advances in Physics*, *55*(3-4), 279–348, 2006.
 - [9] Kato, N., A possible model for large preseismic slip on a deeper extension of a seismic rupture plane, *Earth and Planetary Science Letters*, *216*(1-2), 17–25, 2003.
 - [10] Shibazaki, B., and Y. Iio, On the physical mechanism of silent slip events along the deeper part of the seismogenic zone, *Geophysical Research Letters*, *30*(9), 1489, 2003.
 - [11] Weeks, J. D., Constitutive laws for high-velocity frictional sliding and their influence on stress drop during unstable slip, *Journal of Geophysical Research*, *98*, 17637–17648, 1993.
 - [12] Liu, Y., and J. Rice, Aseismic slip transients emerge spontaneously in three-dimensional rate and state modeling of subduction earthquake sequences, *Journal of Geophysical Research*, *110*(B8), 1–14, 2005.
 - [13] Yoshida, S., and N. Kato, Episodic aseismic slip in a two-degree-of-freedom block-spring model, *Geophysical Research Letters*, *30*(13), 1681, 2003.
 - [14] Ben-David, O., S. M. Rubinstein, and J. Fineberg, Slip-stick and the evolution of frictional strength., *Nature*, *463*(7277), 76–9, 2010.
 - [15] Braun, O., Barel, I., and Urbakh, M., Dynamics of transition from static to kinetic friction, *Physical Review Letters*, *103*, 194301, 2009.
 - [16] Bouchbinder, E., E. A. Brener, I. Barel, and M. Urbakh, Cracklike dynamics at the onset of frictional sliding, arXiv:1103.3942, 2011.
 - [17] Berthoud, P., and T. Baumberger, Shear stiffness of a solid-solid multicontact interface, *Proceedings of the Royal Society of London. Series A: Mathematical, Physical and Engineering Sciences*, *454*(1974), 1615, 1998.
 - [18] Brener, E. A., and Marchenko, V. I., Frictional shear cracks, *Journal of Experimental and Theoretical Physics Letters*, *76*, 211–214, 2002.
 - [19] Shi, Z., Needleman, A., and Ben-Zion, Y., Slip modes and partitioning of energy during dynamic frictional sliding between identical elastic-viscoplastic solids, *International Journal of Fracture*, *162*, 51–67, 2010.
 - [20] Bureau, L., Baumberger, T., and Caroli, C., Shear response of a frictional interface to a normal load modulation, *Physical Review E*, *62*, 6810–6820, 2000.
 - [21] Nakatani, M., and Scholz, C. H., Intrinsic and apparent short-time limits for fault healing: theory, observations, and implications for velocity-dependent friction, *Journal of Geophysical Research* *111*, B12208, 2006.
 - [22] Yang, Z., Zhang, H. P., and Marder, M., Constitutive laws for high-velocity frictional sliding and their influence on stress drop during unstable slip, *Proceedings of the National Academy of Sciences of the United States of America*, *195*, 13264–13268, 2008.
 - [23] Baumberger, T., and P. Berthoud, Physical analysis of the state- and rate-dependent friction law. II. Dynamic friction, *Physical Review B*, *60*(6), 3928–3939, 1999.
 - [24] Kilgore, B. D., Blanpied, M. L., and Dieterich, J. H., Velocity dependent friction of granite over a wide range of conditions, *Geophysical Research Letters*, *20*(10), 903–906, 1993.
 - [25] Heslot, F., T. Baumberger, B. Perrin, B. Caroli, and C. Caroli, Creep, stick-slip, and dry-friction dynamics: Experiments and a heuristic model, *Physical Review E*, *49*(6), 4973–4988, 1994.